Sandwich-structured AgCl@Ag@TiO$_2$ with excellent visible-light photocatalytic activity for organic pollutant degradation and *E. coli* K12 inactivation

Baozhu Tian [a],[*], Rongfang Dong [a], Jingming Zhang [b], Shenyuan Bao [a], Fan Yang [a], Jinlong Zhang [a],[*]

[a] *Key Lab for Advanced Materials and Institute of Fine Chemicals, East China University of Science and Technology, 130 Meilong Road, Shanghai 200237, PR China*
[b] *Department of Pharmacology, School of Pharmacy, Second Military Medical University, 325 Guohe Road, Shanghai 200433, PR China*

ABSTRACT

Sandwich-structured AgCl@Ag@TiO$_2$ plasmonic photocatalyst was synthesized by a facile multistep route, including a controllable double-jet precipitation technique to fabricate cubic AgCl core, a gradual temperature-rise process to coat TiO$_2$ shell layer, and UV light reduction to generate Ag nanoparticles (NPs) between AgCl core and TiO$_2$ shell. The obtained samples were characterized by scanning electron microscopy (SEM), transmission electron microscopy (TEM), X-ray diffraction (XRD), X-ray photoelectron spectroscopy (XPS), and UV–vis diffuse reflectance spectroscopy (DRS). Beneficial from the fact that Ag NPs can respond to visible light and sandwich-structure can effectively separate the photo-generated electrons and holes, AgCl@Ag@TiO$_2$ exhibited excellent visible-light photocatalytic activity not only for the degradations of acid orange 7 and 2,4-dichlorophenol but also for the inactivation of *Escherichia coli* (*E. coli*) K12. The transient photocurrent tests proved that AgCl@Ag@TiO$_2$ sandwich-structure has higher efficiency for the separation of photo-generated electrons and holes than AgCl@Ag core–shell structure. Electron spin resonance (ESR) tests with DMPO and the radical trapping experiments confirmed that $^\bullet$O$_2^-$, $^\bullet$OH and Cl^0 are the reactive species responsible for the degradation of organic pollutants and bacteria.

© 2014 Elsevier B.V. All rights reserved.

1. Introduction

In recent years, with the rapid development of industry, a large amount of industrial wastewater containing various environmental pollutants such as dyes, pharmaceuticals, and even pathogenic microorganisms, has been released into water sources [1,2]. More and more regions around the world are suffering from water supply problems [1,2]. In this context, semiconductor photocatalysis has received increasing attention as a promising solution to solve water pollution problems by decomposing pollutants and bacteria [3–7]. Amongst various semiconductor materials, TiO$_2$ has been widely studied because of its nontoxicity, highly chemical stability, and low cost [8,9]. However, the practical applications of TiO$_2$ have been suppressed by its two drawbacks, one of which is the poor solar efficiency that is determined by its wide band gap; the other is the low quantum yield that arises from the rapid recombination of photo-generated electrons and holes. To solve the problems, the researchers have explored many strategies such as doping with metals [10,11] or non-metals [12,13], deposition of noble metals [14], coupling with other semiconductors [15], and anchoring organic sensitizers [16,17]. However, these efforts still cannot totally meet the requirement of water treatment driven by solar energy.

Silver halides (AgX, X = Cl, Br, I) are well known as photosensitive materials and are widely used in photographic industry. Formerly, AgX materials were considered to be unstable as photocatalysts, due to the fact that they would decompose into Ag when exposed to light. However, the later researches confirmed that Ag nanoparticles (NPs) formed on AgX surface can enhance the stability of AgX under visible light irradiation. This is because the photo-generated electrons would preferentially transfer to Ag Nps rather than the Ag$^+$ ions in AgX [18,19]. Moreover, the Ag NPs anchored on AgX surface can greatly extend the photo-response of photocatalyst in the visible light region by surface plasmon resonance (SPR) [19–26]. As a result, AgX-based plasmonic photocatalysts (denoted as AgX@Ag)

* Corresponding authors. Tel.: +86 21 64252062; fax: +86 21 64252062.
  E-mail addresses: baozhutian@ecust.edu.cn (B. Tian),
jinlongzhang@ecust.edu.cn (J. Zhang).

have received much attention due to their excellent visible-light photocatalytic activity for degrading organic pollutants [19–26].

Recently, some researches proved that AgCl/Ag coupled with TiO_2 showed improved visible-light photocatalytic performance and stability for degrading organic pollutants [27–30]. For instance, Yu et al. [26] prepared TiO_2/AgCl/Ag nanotube arrays (NTs) by depositing AgCl nanoparticles (NPs) on TiO_2 nanotube arrays and further photo-reduction. It was found that the obtained TiO_2/AgCl/Ag NTs photocatalyst exhibited excellent visible-light photocatalytic activity and stability for the degradation of methyl orange. Dai et al. [29] prepared TiO_2/AgCl/Ag by deposition-precipitation and photo-reduction method. They found that this composite photocatalyst exhibited efficient visible-light photo-catalytic activity for the degradation of 4-chlorophenol and the reduction of Cr (VI) ions. The outstanding visible-light photo-catalytic performance should be attributed to the co-operations of Ag NPs and composite structure, in which the Ag NPs is in charge of visible light absorption while the composite structure is responsible for the separation of photo-generated electrons and holes. However, for these composite photocatalysts, the less stable AgCl was usually exposed to external environment, inevitably resulting in chemical corrosion and the deterioration of stability. Therefore, fabricating TiO_2 and AgCl composite materials with both high photocatalytic activity and stability is necessary for both researches and applications. Additionally, the bactericidal properties of Ag/AgBr/TiO_2 and AgI/TiO_2 have been studied [1,31], but as far as we know, the bactericidal activity of AgCl/Ag/TiO_2 is still unclear. Moreover, it is also urgent to further clarify the reactive species in AgX/TiO_2 system responsible for the degradation of organic pollutants and bacteria.

In this study, we fabricated sandwich-structured AgCl@Ag@TiO_2 composite photocatalyst by a facile multistep route, in which a double-jet precipitation technique was employed to construct cubic AgCl core, a hydrothermal precipitation method was used to coat TiO_2 shell layer, and UV light reduction was conducted to form Ag NPs between AgCl core and TiO_2 shell. The microstructures and optical properties of the obtained samples were investigated by the means of scanning electron microscopy (SEM), transmission electron microscopy (TEM), X-ray diffraction (XRD), X-ray photoelectron spectroscopy (XPS), and UV–vis diffuse reflectance spectroscopy (DRS). The photocatalytic activity of AgCl@Ag@TiO_2 for decomposing organic pollutants was evaluated in terms of the degradations of acid orange 7 (AO7) and 2,4-dichlorophenol (2,4-DCP), whereas its bactericidal activity was tested using *Escherichia coli* (*E. coli*) K12 as a model bacterium. On the basis of photo-current measurements, radical trapping experiments, and electron spin resonance (ESR) tests with 5,5-dimethyl-1-pyrroline *N*-oxide (DMPO), the photocatalytic reaction mechanism of AgCl@Ag@TiO_2 was proposed.

2. Experimental

2.1. Preparation of AgCl@Ag@TiO_2 sandwich-structured photocatalyst

Cubic AgCl grains were prepared by a controllable double-jet precipitation technique according to our previous report [23]. Under magnetic stirring, 2.9 g of AgCl grains were dispersed in 50 mL of gelatin aqueous solution and the pH was adjusted to 2.0 with diluted H_2SO_4 solution. Subsequently, 2.97 g of $Ti(SO_4)_2$ was added to the suspension in batches, followed by a temperature-rise process from 30 °C to 80 °C. Then, the suspension was transferred into a Teflon-inner-liner stainless autoclave and kept at 120 °C for 12 h. When the reactor was cooled to room temperature, the

sample was separated by centrifugation, washed with deionized water, and dried at the room temperature.

UV light reduction was employed to form Ag NPs on the surface of AgCl. In a typical procedure, 0.5 g of AgCl@TiO_2 powder was put into a quartz tube containing 100 mL of water and irradiated with a 150 W high-pressure Hg lamp ($\lambda_{max} = 365$ nm) for 2 h under stirring. Finally, the precipitate was collected by centrifugation and denoted as AgCl@Ag@TiO_2. For comparison, AgCl@Ag was prepared by photo-reducing AgCl powder with the same method, while N-doped TiO_2 was prepared according to the previous report [32].

2.2. Characterization

The morphologies of the samples were observed on a JEOL JSM-6360 LV scanning electron microscopy (SEM) and a JEM-1200 EX II transmission electron microscopy. X-ray diffraction (XRD) measurements were carried out with a Rigaku D/max 2550 VB/PC X-ray diffractometer using Cu Ka radiation ($\lambda = 0.154056$ nm). The X-ray photoelectron spectroscopy (XPS) analyses were carried out on a Perkin-Elmer PHI 5000 Versaprobe system with Al K1 radiation at 300 W. The UV–vis diffuse reflectance spectra were measured with a SHIMADZU UV-2450 spectroscopy equipped with an integrating sphere assembly, using $BaSO_4$ as the reference material. ESR spectra were obtained using a Bruker EMX-8/2.7C electron paramagnetic resonance spectrometer equipped with a Quanta-Ray Nd:YAG laser system as the irradiation source ($\lambda \geq 532$ nm).

2.3. Photocatalytic activity measurement

The photocatalytic activities of the prepared photocatalysts were evaluated in terms of the degradations of acid orange 7 (AO7) dye and 2,4-dichlorophenol (2,4-DCP). The photocatalytic reactions were conducted under visible light irradiation by using a 500 W halogen tungsten lamp with a UV cut-off filter ($\lambda \geq 420$ nm) as light source. For each measurement, 60 mg of photocatalyst sample was added into a quartz tube containing 100 mL of AO7 aqueous solution (20 mg L^{-1}) or 2,4-DCP (40 mg L^{-1}). Prior to light irradiation, the suspension was sonicated for 10 min and stirred for 30 min in the dark to attain the adsorption–desorption equilibrium for AO7 or 2,4-DCP. At a given time interval, about 4 mL of suspension was withdrawn, centrifuged, and filtered to remove the remained particles. The residual concentrations of AO7 and 2,4-DCP were detected with a SHIMADZU UV-2450 UV–vis spectrophotometer and a CTO-10 ASVP high-performance liquid chromatograph, respectively.

2.4. Bactericidal activity test

The bactericidal activities of the samples were evaluated in terms of the inactivation of gram-negative bacterium *Escherichia coli* K12 (*E. coli* K12) in 0.9% saline under visible light irradiation. The tests were conducted according to the following procedures. Firstly, *E. coli* K12 bacteria were incubated in a Luria–Bertani (LB) nutrient solution at 37 °C for 24 h under shaking, and washed with 0.9% saline by centrifugation at 4000 rpm. Subsequently, the treated bacteria were re-suspended and diluted in gradient to 2×10^7 colony-forming units (CFU/mL) with 0.9% saline. Then, 0.3 mL of diluted cell suspension and 60 mg of photocatalyst were added into a conical beaker containing 30 mL of 0.9% saline. A 300 W Xe arc lamp (CEL-HXF300) with a UV cut-off filter ($\lambda \geq 420$ nm) was used as light source and the light was focused onto the beaker reactor. All of the bactericidal experiments were carried out under magnetic stirring at room temperature. At a given time interval, an aliquot of the suspension was immediately diluted with 0.9% saline and uniformly dispersed onto an incubated nutrient agar plate. Finally, the bacterium colonies were counted to
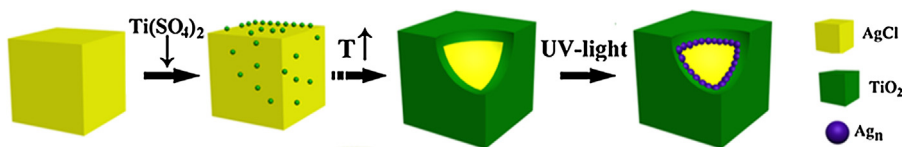
Scheme 1. Synthetic route of the sandwich-structured AgCl@Ag@TiO$_2$ plasmonic photocatalyst.

determine the number of viable cells. Specially, it should be noted that all materials including the photocatalysts used in the experiments were autoclaved at 121 °C for 20 min to ensure sterility.

2.5. Photocurrent measurement

To evaluate the photoelectric efficiencies of the samples, photocurrents were measured by an electrochemical analyzer (AMETEK Princeton Applied Research, Uersastat 7) in a standard three-electrode system using the sample as the working electrode with an active area of 8 cm^2, a Pt foil as the counter electrode, a saturated calomel electrode (SCE) as the reference electrode, and 0.1 M Na$_2$SO$_4$ as the electrolyte. A 300 W Xe arc lamp with a UV cutoff filter ($\lambda \geq 420$ nm) was used as the visible light source.

3. Results and discussion

3.1. Characterization of catalysts

Scheme 1 illustrates the synthetic route of AgCl@Ag@TiO$_2$ sandwich-structured photocatalyst. Firstly, uniform AgCl cubic grains were prepared by a controllable double-jet precipitation process. Secondly, TiO$_2$ shell layer was deposited onto the surface of AgCl via the hydrolysis of Ti(SO$_4$)$_2$ in the presence of gelatin dispersant. Finally, some Ag ions in the surface region of AgCl were reduced to Ag NPs by UV light illumination. In these processes, there are two key steps that determine whether or not TiO$_2$ can be uniformly coated on the surface of AgCl grains. One is to adjust the pH value of AgCl suspension using dilute H$_2$SO$_4$, which can effectively slow down the hydrolysis rate of Ti(SO$_4$)$_2$ and make hydrolyzed titanium uniformly deposit on AgCl surface. Otherwise, only part of TiO$_2$ can be deposited onto AgCl surface (Supporting Information, Fig. S1). The other is the gradual temperature-rise process, which can effectively control the hydrolysis rate of Ti(SO$_4$)$_2$, or else, a mass of TiO$_2$ would aggregate together (Supporting Information, Fig. S2).

Fig. 1A shows the SEM image of the as-prepared AgCl grains. It can be seen that all AgCl grains exhibited regular cubic morphology with side length of 0.7 μm. After hydrothermal treatment, AgCl grains were uniformly wrapped by TiO$_2$ nanoparticles, forming AgCl@TiO$_2$ core–shell structure (Fig. 1B). As shown in Fig. 1C, AgCl@Ag@TiO$_2$ remained the profile of its precursor AgCl@TiO$_2$, demonstrating that the formation of Ag nanoparticles between AgCl core and TiO$_2$ shell does not change the morphology of AgCl@TiO$_2$. Fig. 2A and B shows the TEM images of AgCl@TiO$_2$ bombed by electron beams for 2 min and 10 min, respectively. It can be seen that the boundary between AgCl core and TiO$_2$ shell became discernable after electron bombardment for 10 min (Fig. 2A). Under high-energy electron irradiation, AgCl is unstable and can convert into metallic Ag, leading to the shrinkage of AgCl core and the formation of yolk–shell structure. To further investigate the thickness of TiO$_2$ shell and the structure of interfacial Ag, we treated AgCl@TiO$_2$ and AgCl@Ag@TiO$_2$, respectively, with Na$_2$S$_2$O$_3$ solution. It can be seen that AgCl can be totally removed and the thickness of TiO$_2$ coating was about 0.1 μm. As shown in Fig. 2D, the interfacial Ag showed spherical or irregular morphologies with sizes varying from 30 nm to 150 nm.
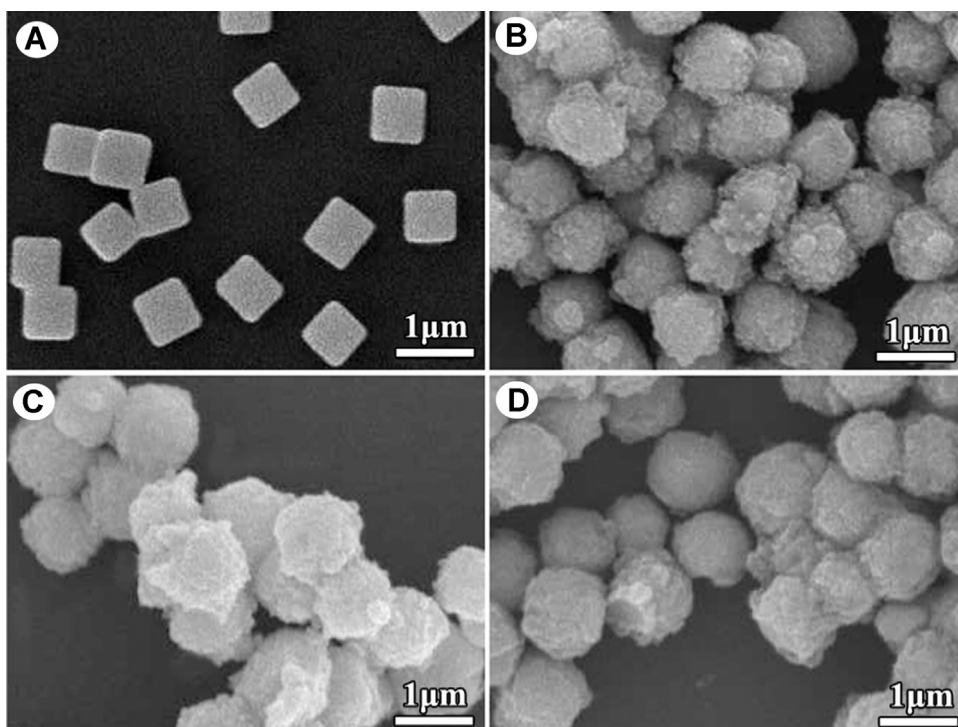

Fig. 1. SEM images of (A) AgCl, (B) AgCl@TiO$_2$, (C) AgCl@Ag@TiO$_2$, and (D) AgCl@Ag@TiO$_2$ after seven cycles of degrading AO7.
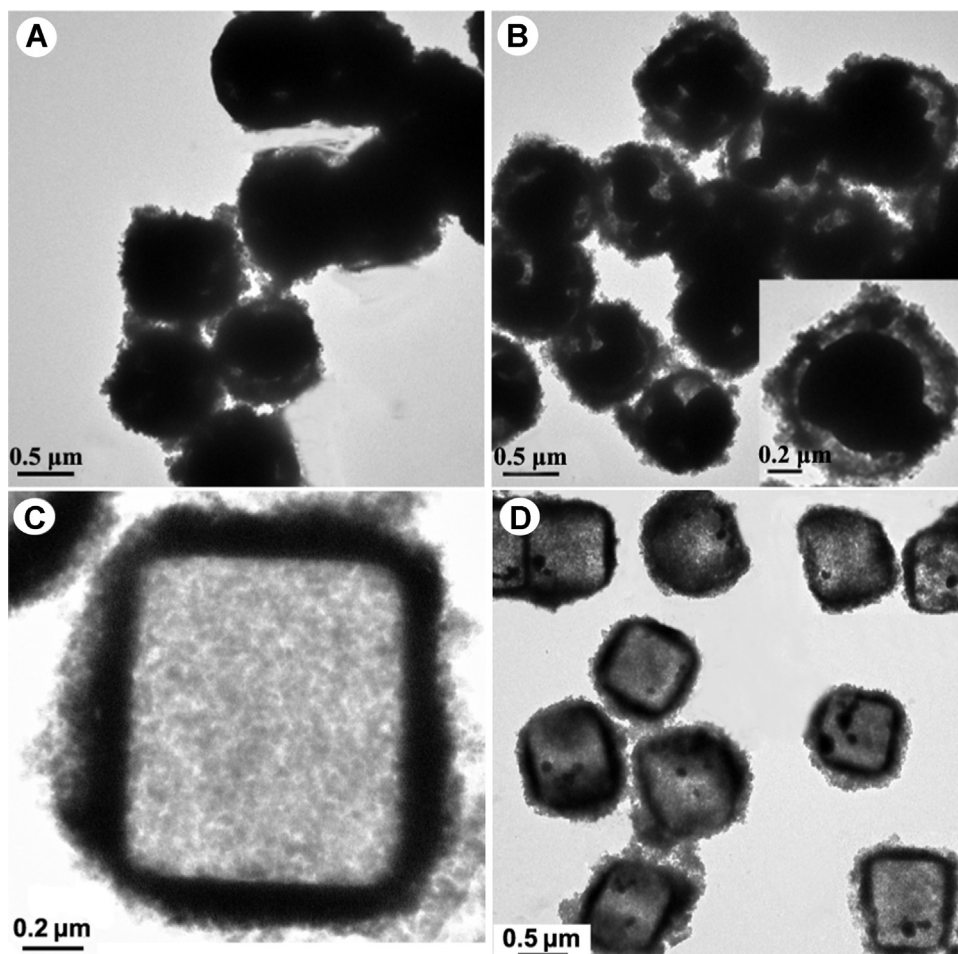
Fig. 2. TEM images of AgCl@TiO$_2$ bombed by electron beams for (A) 2 min and (B) 10 min. TEM images of (C) AgCl@TiO$_2$ and (D) AgCl@Ag@TiO$_2$ treated with Na$_2$S$_2$O$_3$ solution.

Fig. 3 shows the XRD patterns of AgCl, AgCl@Ag, AgCl@TiO$_2$, and AgCl@Ag@TiO$_2$. All samples showed very approximate diffraction peaks at $2\theta = 27.8°$, $32.2°$, $46.2°$, $54.8°$, $57.5°$, and $76.7°$, which should be indexed to AgCl (1 1 1), (2 0 0), (2 2 0), (3 1 1), (2 2 2), and (4 2 0) plane reflections, respectively (JCPDS file: 31-1238). The inset of Fig. 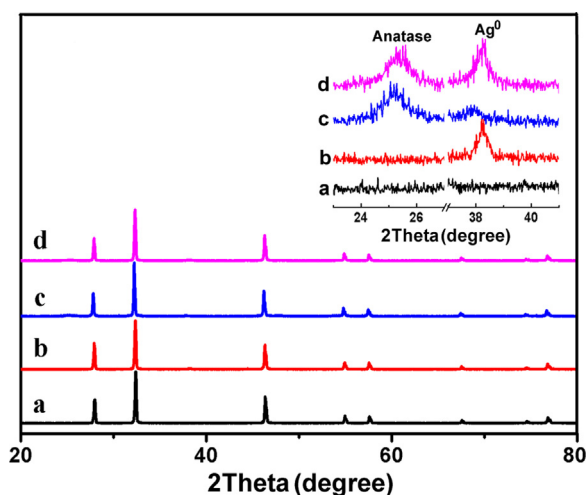3 shows the enlarged patterns of these samples in the ranges of $2\theta = 23–27°$ and $37–41°$. Compared with AgCl and AgCl@Ag, AgCl@TiO$_2$ and AgCl@Ag@TiO$_2$ exhibited additional peaks at $2\theta = 25.3°$, which should be ascribed to anatase TiO$_2$ (1 0 1) plane reflection (JCPDS file: 21-1272), confirming the formation of anatase TiO$_2$ shell layer. Additionally, both AgCl@Ag and AgCl@TiO$_2$ showed weak peaks around the scattering angle of $2\theta = 38.2°$, corresponding to the cubic phase Ag (1 1 1) plane (JCPDS file: 65-2871). Other Ag characteristic peaks can also be discernable, as shown in Fig. S3 (Supporting Information). This result indicated that UV light reduction is a competent technique for producing Ag NPs on AgCl surface. The average particle size of Ag particles in AgCl@Ag@TiO$_2$ was calculated by applying the Debye–Scherrer formula on the Ag (1 1 1) peak to be 18.2 nm. This size seems to be smaller than that observed by TEM, which may be because the smaller Ag nanoparticles in TEM image are hard to be observed.

The elemental composition and surface chemical status of AgCl@Ag@TiO$_2$ were analyzed by X-ray photoelectron spectroscopy (XPS). In Fig. 4A, the two peaks located at 464.0 and 458.3 eV should be assigned to Ti 2p$_{1/2}$ and Ti 2p$_{3/2}$, respectively [33]. As shown in Fig. 4B, the O1s spectrum is wide and asymmetric, implying that O element at least has two kinds of chemical states. According to the previous reports [33,34], the O 1s peak could be fitted into three peaks at 529.5 eV, 531.2 eV, and 532.8 eV, ascribed to lattice oxygen of TiO$_2$ (O$_L$), adsorbed –OH groups (O$_{OH}$), and H$_2$O (O$_{H_2O}$), respectively. Ag 3d and Cl 2p spectra can be clearly detected by XPS (Fig. 4C and D), indicating that there are some exposed sites among TiO$_2$ particles or the coating thickness somewhere (the joints among TiO$_2$ particles) is very thin. As shown in Fig. 3c, the Ag

Fig. 3. XRD patterns of AgCl (a), AgCl@Ag (b), AgCl@TiO$_2$ (c), and AgCl@Ag@TiO$_2$ (d). The inset is the enlarged patterns in the ranges of $2\theta = 23–27°$ and $37–41°$.
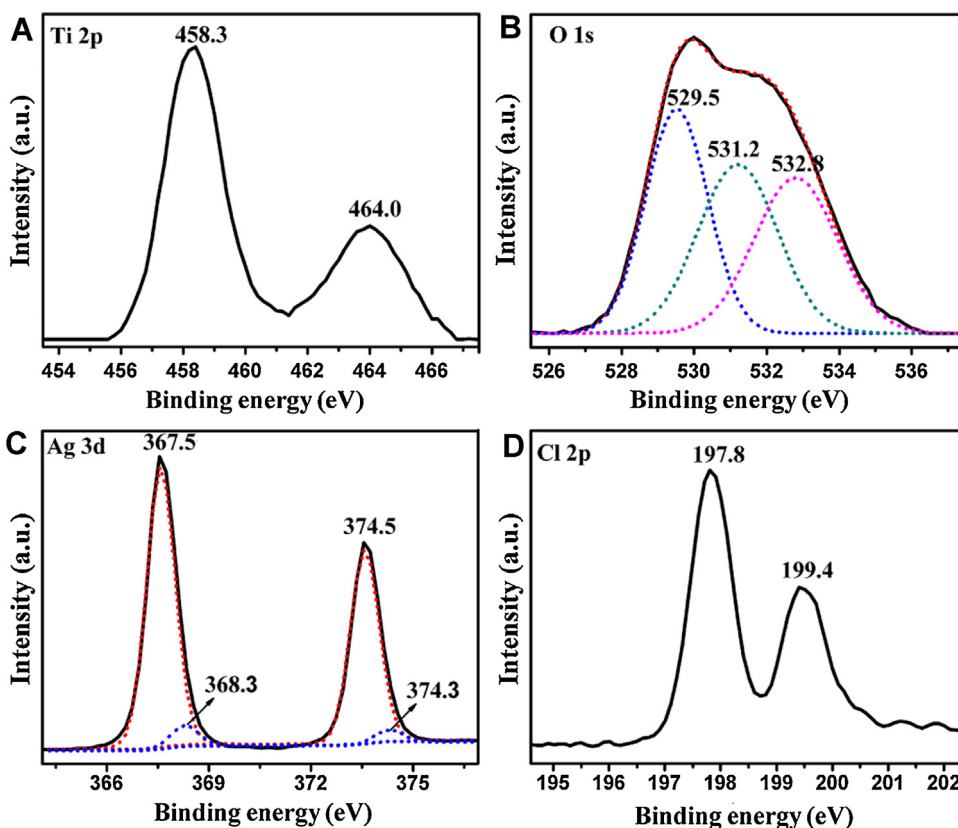
Fig. 4. XPS spectra of AgCl@Ag@TiO$_2$: (A) Ti 2p, (B) O 1s, (C) Ag 3d, and (D) Cl 2p.

3d peaks can be fitted into two sets of double peaks. According to the previous reports [35,36], the peaks at 367.5 and 373.5 eV should be attributed to Ag 3d$_{5/2}$ and Ag 3d$_{3/2}$ of Ag$^+$ in AgCl, whereas the peaks at 368.3 eV and 374.3 eV should be ascribed to Ag 3d$_{5/2}$ and Ag 3d$_{3/2}$ of metallic Ag. In Fig. 4D, the double peaks located at 197.8 eV and 199.4 eV can be assigned to the characteristic doublets of Cl 2p$_{3/2}$ and Cl 2p$_{1/2}$, respectively [23,25,35].

The light absorption properties of AgCl, AgCl@TiO$_2$, AgCl@Ag, and AgCl@Ag@TiO$_2$ were analyzed by UV – vis diffuse reflectance spectroscopy. As shown in Fig. 5a, AgCl exhibited two absorption peaks around 230 and 300 nm, ascribed to the direct and indirect exciton transitions of AgCl, respectively [23]. Compared with AgCl and AgCl@Ag, AgCl@TiO$_2$ and AgCl@Ag@TiO$_2$ showed stronger light absorption in the range of 200–400 nm, which is related to the strong UV light absorption of TiO$_2$ (Fig. 5a–d). Because of the surface

plasmon resonance of Ag NPs, both AgCl@Ag and AgCl@Ag@TiO$_2$ displayed remarkable absorption enhancement in the visible light region.

3.2. Photocatalytic activity of degrading organic pollutants and bacteria

The photocatalytic activity of the obtained plasmonic photocatalyst AgCl@Ag@TiO$_2$ was evaluated in terms of the degradations of AO7 dye and 2,4-DCP under visible light irradiation ($\lambda \geq 420$ nm). For comparison, the photocatalytic degradation experiments over N-doped TiO$_2$ (N−TiO$_2$) and AgCl@Ag were also conducted under the same conditions. The degradation curves of AO7 and 2,4-DCP as a function of visible light irradiation time are plotted in Fig. 6A and B, respectively, in which C_0 is the concentration of AO7 (or 2,4-DCP) after adsorption–desorption equilibrium while C represents the corresponding pollutant concentration at a certain time interval. From Fig. 6A, it can be seen that, after visible-light irradiation for 20 min, the degradation rate of AO7 over AgCl@Ag@TiO$_2$ reached 98%, whereas it was only 69% over AgCl@Ag and 7% over N−TiO$_2$. It has been reported that some dyes can be degraded under visible-light irradiation by a self-photosensitization mechanism [15]. To eliminate the influence of dye self-photosensitization, we further selected 2,4-DCP, which has no absorption in the visible-light region, as a model pollutant to evaluate the photocatalytic activity of the above samples. As shown in Fig. 6B, after visible light irradiation for 60 min, 94% of 2,4-DCP was degraded over AgCl@Ag@TiO$_2$, whereas the extent of 2,4-DCP degradation was 74% over AgCl@Ag and 14% over N−TiO$_2$. Because AgCl do not absorb visible light, it is reasonable to ascribe the remarkable visible photocatalytic activity of AgCl@Ag to the contribution of Ag SPR.
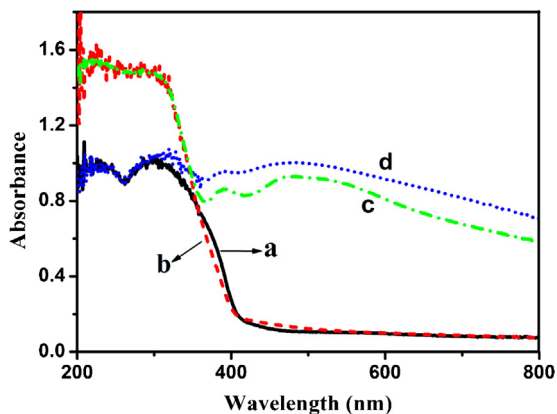

Fig. 5. UV–vis diffuse reflectance spectra of (a) AgCl, (b) AgCl@TiO$_2$, (c) AgCl@Ag, and (d) AgCl@Ag@TiO$_2$.
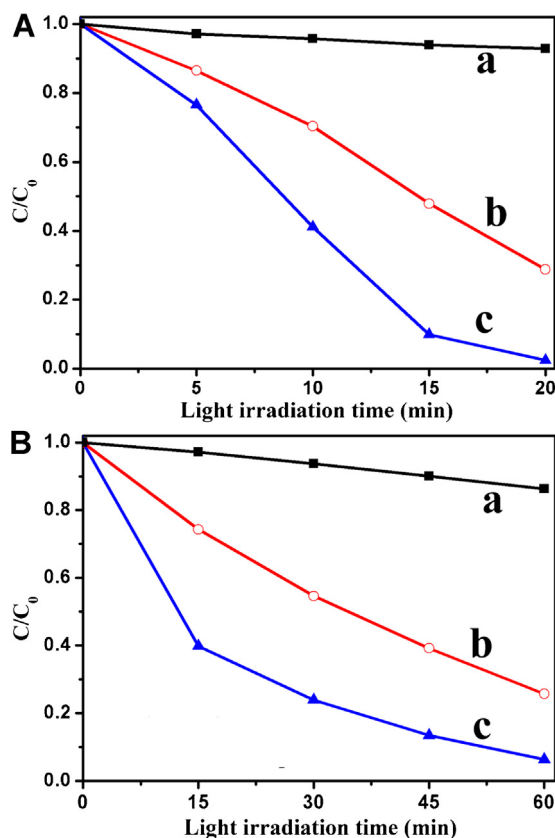
Fig. 6. Photocatalytic degradation curves of (A) AO7 and (B) 2,4-DCP over (a) N–TiO$_2$, (b) AgCl@Ag, and (c) AgCl @Ag@ TiO$_2$.

The photocatalytic bactericidal property of the samples was evaluated by analyzing the number of the surviving *E. coli* K12 bacterium colonies after visible light irradiation ($\lambda \geq 420$ nm). Fig. 7 displays the evolution processes of the surviving *E. coli* colonies over N–TiO$_2$, AgCl@Ag, and AgCl@Ag@TiO$_2$. To accurately measure the bactericidal properties of the photocatalyst samples, two control experiments, i.e., one with photocatalyst but without light and the other with light but without photocatalyst, were also conducted. As shown in Fig. 7, the number of *E. coli* colonies almost had no change without light irradiation, indicating that AgCl@Ag@TiO$_2$ is incapable of killing bacteria without the
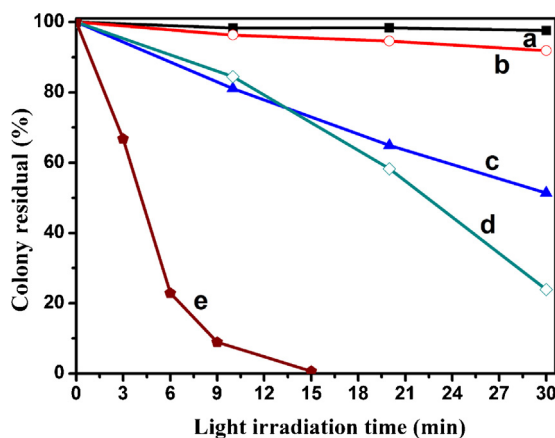

Fig. 7. Photocatalytic inactivation efficiencies of *E. coli* under different conditions: (a) with AgCl@Ag@TiO$_2$ but without light; (b) direct photolysis without photocatalyst; (c) with N–TiO$_2$ and visible light irradiation; (d) with AgCl@Ag and visible light irradiation; (e) with AgCl@Ag@TiO$_2$ and visible light irradiation.
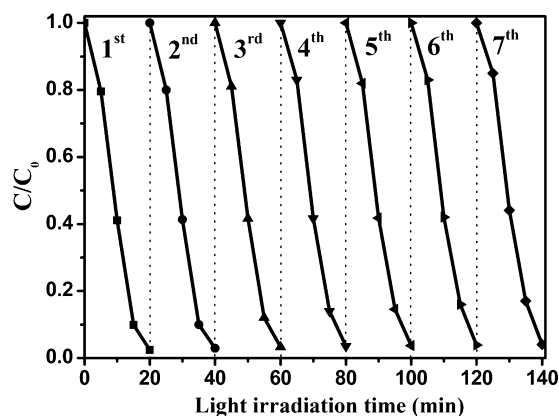

Fig. 8. Cycling runs in the photocatalytic degradation of AO7 over AgCl@Ag@TiO$_2$.

assistance of light. Without photocatalyst, only 6% of *E. coli* K12 was inactivated under visible light irradiation for 30 min (Fig. S4, Supporting Information), suggesting that direct photo-killing is a very slow bactericidal process. In contrast, all of N–TiO$_2$, AgCl@Ag, and AgCl@Ag@TiO$_2$ exhibited evidently improved bactericidal activity (Fig. 7c–e), which is attributed to the contribution of photocatalytic inactivation. After visible light irradiation for 30 min, the inactivation rates of *E. coli* K12 over N–TiO$_2$ and AgCl@Ag were 48.6% and 76.0%, respectively. As a comparison, when AgCl@Ag@TiO$_2$ was used, about 77% of *E. coli* K12 was inactivated after visible light irradiation for only 6 min, and almost all *E. coli* was killed within 15 min, as displayed in Fig. 8 and Fig. S5 (Supporting Information). The excellent bactericidal activity of AgCl@Ag@TiO$_2$ is probably beneficial from its special heterojunction structure. It is generally accepted that the inactivation of *E. coli* K12 is caused by the oxidative species (e.g., $^{\bullet}O_2{}^{-}$) generated on photocatalyst surface under light irradiation, which could oxidize the cell membranes and afterwards kill the bacteria [1,37].

As photostability is very important to a photocatalyst for its practical applications, the photostability of AgCl@Ag@TiO$_2$ was investigated by cycle degradation experiments. As shown in Fig. 8, the photocatalytic efficiency of AgCl@Ag@TiO$_2$ had no obvious loss even after seven cycles of degrading AO7. The SEM image in Fig. 1D confirmed that the morphological structure of AgCl@Ag@TiO$_2$ also kept unchanged after cycle degradation tests. These results demonstrated that AgCl@Ag@TiO$_2$ is a highly stable photocatalyst under visible light irradiation.

3.3. Reaction mechanism

Semiconductor photocatalytic reactions include four basic processes, i.e., charge carrier generation, charge trapping, charge recombination, and interfacial charge transfer [38], which determine the final photocatalytic performance of a photocatalyst. The result that AgCl@Ag@TiO$_2$ exhibited excellent visible-light photocatalytic activity is probably ascribed to the special AgCl–Ag–TiO$_2$ sandwich structure, in which Ag NPs are responsible for the visible-light absorption, while AgCl and TiO$_2$ act as hole and electron collectors, respectively. Photoelectrochemical measurements are often used to qualitatively study the excitation and transfer of photo-generated charge carriers in photocatalysts [39–42]. Here, we measured the transient photocurrent responses of AgCl@Ag and AgCl@Ag@TiO$_2$ to identify the effect of sandwich structure on charge separation. Fig. 9 displays the photocurrent–time (*I–t*) curves of the above two samples with typical on–off cycles of intermittent visible light irradiation. As seen from the figure, the photocurrent boosted rapidly once the light was turned on and remained a constant value during the light was on. And then,
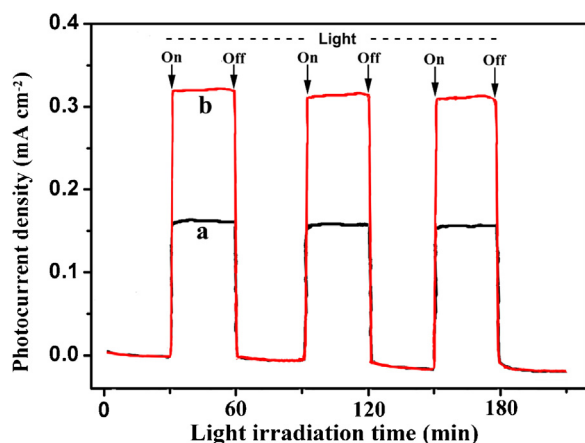
Fig. 9. Transient photocurrent responses of (a) AgCl@Ag and (b)AgCl@Ag@TiO$_2$ under visible light irradiation.
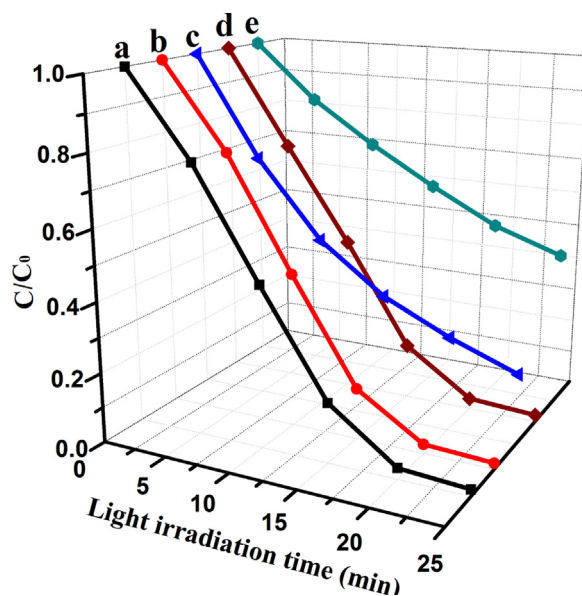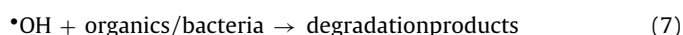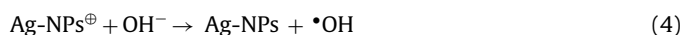

Fig. 10. Photocatalytic degradation curves of AO7 over AgCl@Ag@TiO$_2$ catalyst under different conditions: (a) no scavenger, (b) 10 mM tertiary butanol, (c) 10 mM NaHCO$_3$, (d) 0.05 mM NaOH, and (e) 0.1 mM p-benzoquinone.

it instantaneously declined to zero as long as the light was cut off. The initial current is due to the separation of electron–hole pairs at the semiconductor/electrolyte interface: holes are trapped by the reduced species in the electrolyte, while electrons are transported to the back contact substrate [39,40]. Since both AgCl and TiO$_2$ are incapable of absorbing visible light, the production of photocurrent should result from Ag SPR. Apparently, sandwich-structured AgCl@Ag@TiO$_2$ exhibited much higher transient photocurrent density than AgCl@Ag under visible light irradiation, which is beneficial from the efficient separation of photo-generated electrons and holes.

It is generally accepted that organic pollutants (or bacteria) can be degraded by photocatalytic oxidation processes, in which a series of photo-induced reactive species, such as h$^+$, $^\bullet$OH, and $^\bullet$O$_2{}^-$, are involved in the degradation reaction of organic pollutants (or bacteria). To elucidate the main reactive species responsible for the degradation of organic pollutants (or bacteria) over AgCl@Ag@TiO$_2$ photocatalyst, a series of quenchers were employed to scavenge the corresponding reactive species. Here, methanol was used to quench $^\bullet$OH in the solution, NaHCO$_3$ for h$^+$ and $^\bullet$OH adsorbed on the photocatalyst surface, and p-benzoquinone for $^\bullet$O$_2{}^-$ [43]. By comparing Fig. 10a and b, it can be confirmed that tertiary butanol quencher almost had no influence on AO7 degradation. In the presence of NaHCO$_3$, the degradation rate obviously decreased, which is much higher than the influence of NaOH (Fig. 10c and d), indicating that the change of pH is not the reason that results in the depression of photocatalytic activity. Therefore, h$^+$ and $^\bullet$OH adsorbed on the photocatalyst surface probably are the main active species responsible for the degradation of organic pollutants (or bacteria). As shown in Fig. 10e, the introduction of p-benzoquinone significantly restrained the degradation of AO7, suggesting that $^\bullet$O$_2{}^-$ plays a key role in the degradation reactions.

To further ascertain the active species over AgCl@Ag@TiO$_2$ photocatalyst, the ESR spin-trap tests with 5,5-dimethyl-1-pyrroline N-oxide (DMPO) were carried out. Under visible light irradiation, a quartet with peak intensity ratio of 1:2:2:1 was detected, consistent with the characteristic peaks of $^\bullet$OH adduct [44,45]. In contrast, no such signals were detected in dark (Fig. 11A). Due to the fact that $^\bullet$O$_2{}^-$ radicals in water are very unstable and undergo rapid disproportionation rather than slowly react with DMPO [45,46], DMPO–$^\bullet$O$_2{}^-$ adduct over TiO$_2$@AgCl@Ag was detected in methanol dispersion. As shown in Fig. 11B, a sextet with similar peak intensity was produced under visible light irradiation, which should be ascribed to the characteristic peaks of DMPO–$^\bullet$O$_2{}^-$ adduct [44,45]. This result confirmed that $^\bullet$O$_2{}^-$ radicals are important reactive species in the degradation reaction, consistent with Fig. 10e. In the
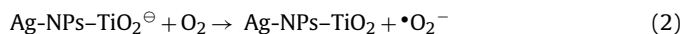
case of $^\bullet$OH, the appearance of DMPO–$^\bullet$OH seemed to be in conflict with the result of quencher trapping experiment. However, when AO7 was added to the reaction system, the characteristic quartet was replaced by a new sextet. Apparently, the new sextet is different to that of DMPO–$^\bullet$O$_2{}^-$, probably resulting from the adduct product of AO7 with $^\bullet$OH. The speed of addition reaction between AO7 and $^\bullet$OH is faster than that between DMPO and $^\bullet$OH so that the characteristic quartet ascribed to DMPO–$^\bullet$OH was replaced by the new sextet when AO7 was added. This also can explain the fact that the addition of tertiary butanol did not change the degradation rate of AO7 (Fig. 10b).

The proposed reaction mechanism in AgCl@Ag@TiO$_2$ photocatalytic system for the degradation of organic pollutants (or bacteria) is schematically illustrated in Fig. 12. Under visible light irradiation, Ag NPs produce electrons and holes, which can be separated by the SPR-induced local electromagnetic field (Eq. (1)) [20,47]. According to the previous report [48], the conduction band (CB) and valence band (VB) edges of AgCl (−3.3 eV and −6.6 eV) are higher than those of TiO$_2$ (−4.0 eV and −7.2 eV), respectively. Due to the suitable CB and VB energy levels of AgCl and TiO$_2$, the photo-generated electrons transfer to TiO$_2$ while holes transfer to AgCl, thus, the electrons and holes can be separated. Then, the electrons are trapped by adsorbed O$_2$ to form $^\bullet$O$_2{}^-$ (Eq. (2)), while the holes combine with OH$^-$/or Cl$^-$ ions to form $^\bullet$OH/or Cl^0 radicals (Eqs. (3) and (4)). All of $^\bullet$O$_2{}^-$, $^\bullet$OH, and Cl^0 are reactive species responsible for the degradation of organic pollutants (or bacteria) (Eqs. (5)–(7)). The special sandwich structure can effectively separate photo-generated electrons and holes, favorable to the improvement of photocatalytic activity.
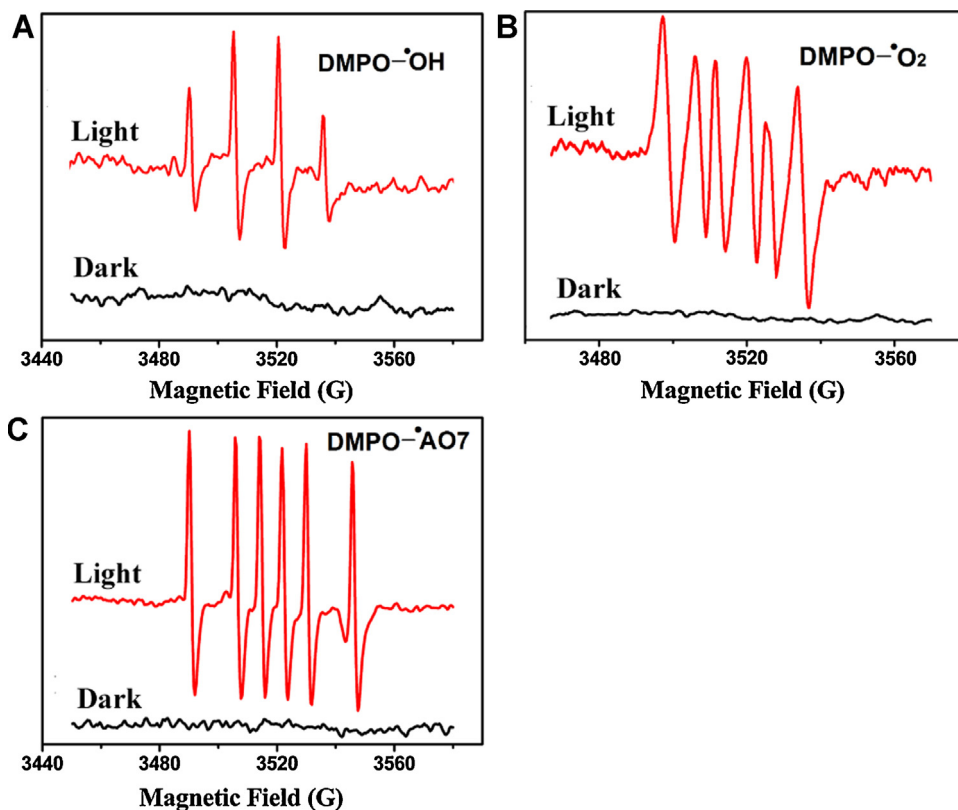
$$\text{Ag-NPs} + h\nu \rightarrow \text{Ag-NPs}^* \rightarrow \text{Ag-NPs}^\ominus + \text{Ag-NPs}^\oplus \qquad (1)$$

$$\text{Ag-NPs–TiO}_2{}^\ominus + \text{O}_2 \rightarrow \text{Ag-NPs–TiO}_2 + {}^\bullet\text{O}_2{}^- \qquad (2)$$

$$\text{Ag-NPs}^\oplus + \text{Cl}^- \rightarrow \text{Ag-NPs} + \text{Cl}^0 \qquad (3)$$

$$\text{Ag-NPs}^\oplus + \text{OH}^- \rightarrow \text{Ag-NPs} + {}^\bullet\text{OH} \qquad (4)$$

$$\text{Cl}^0 + \text{organics/bacteria} \rightarrow \text{degradation products} + \text{Cl}^- \qquad (5)$$

$${}^\bullet\text{O}_2{}^- + \text{organics/bacteria} \rightarrow \text{degradation products} \qquad (6)$$

$${}^\bullet\text{OH} + \text{organics/bacteria} \rightarrow \text{degradation products} \qquad (7)$$

Fig. 11. DMPO spin-trapping ESR spectra recorded at ambient temperature with AgCl@Ag@TiO$_2$ photocatalyst in (A) aqueous dispersion (for DMPO−•OH), (B) methanol dispersion (for DMPO−•O$_2$⁻), and (C) AO7 aqueous dispersion under visible light irradiation ($\lambda \geq 420$ nm).
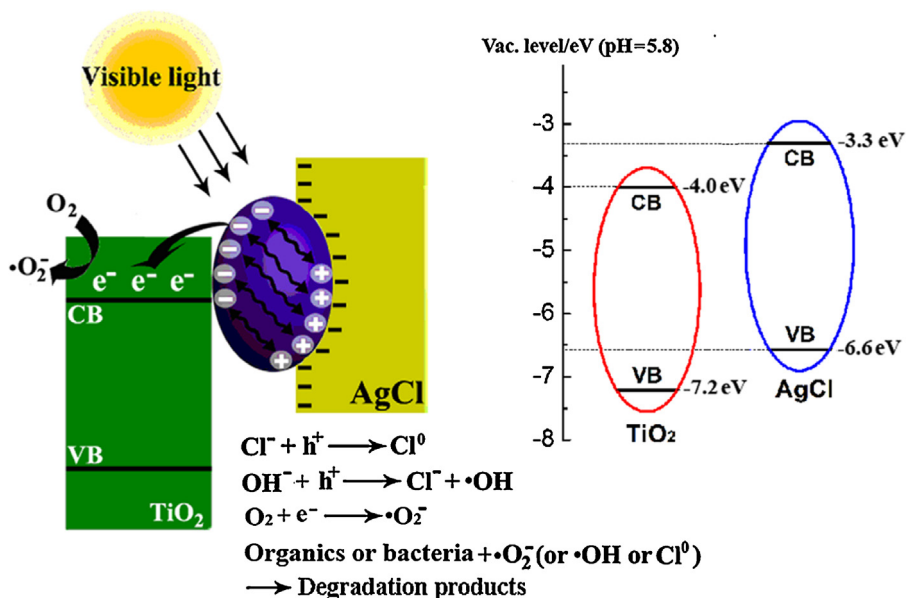

Fig. 12. Proposed reaction mechanism of organics (or bacteria) over AgBr@Ag@TiO$_2$ photocatalyst under visible light irradiation.

4. Conclusions

In this study, we prepared sandwich-structured AgCl@Ag@TiO$_2$ plasmonic photocatalyst by a versatile multistep route, in which a controllable double-jet precipitation technique was used to synthesize cubic AgCl core, a low-temperature precipitation method was introduced to coat TiO$_2$ shell layer, and a light reduction process was performed to generate Ag nanoparticles (NPs) between

AgCl core and TiO$_2$ shell. In the low-temperature precipitation process, both low pH and gradual temperature-rise process are necessary for the formation of uniform TiO$_2$ shell layer. The sandwich-structured AgCl@Ag@TiO$_2$ photocatalyst showed excellent photocatalytic activity in terms of the degradations of acid orange 7 dye and 2,4-dichlorophenol as well as the inactivation of *E. coli* K12, which is because Ag nanoparticles can respond to visible light while the sandwich structure facilitates the separation of

photo-generated electrons and holes. The transient photocurrent tests proved that the sandwich structure is more favorable to the separation of photo-generated electrons and holes when compared to AgCl@Ag core–shell structure. The radical trapping experiments and electron spin resonance (ESR) tests with DMPO confirmed that $\cdot O_2^-$, $\cdot OH$ and Cl^0 are the reactive species responsible for the degradation of organic pollutants and the inactivation of bacteria. As a highly efficient photocatalyst, the sandwich-structured AgCl@Ag@TiO$_2$ plasmonic photocatalyst can be potentially applied in wastewater treatment, sterilization, and other photocatalytic fields.

Acknowledgements

Appendix A. Supplementary data

Supplementary data associated with this article can be found, in the online version, at http://dx.doi.org/10.1016/j.apcatb.2014.04.008.

References

[1] Y. Hou, X.Y. Li, Q.D. Zhao, G.H. Chen, C.L. Raston, Environ. Sci. Technol. 46 (2012) 4042–4050.
[2] M.A. Shannon, P.W. Bohn, M. Elimelech, J.G. Georgiadis, B.J. Marinas, A.M. Mayes, Nature 452 (2008) 301–310.
[3] I.K. Konstantinou, T.A. Albanis, Appl. Catal. B 49 (2004) 1–14.
[4] M. Pelaez, N.T. Nolan, S.C. Pillai, M.K. Seery, P. Falaras, A.G. Kontos, P.S.M. Dunlop, J.W.J. Hamilton, J.A. Byrne, K. O'Shea, M.H. Entezari, D.D. Dionysiou, Appl. Catal. B 125 (2012) 331–349.
[5] M.N. Chong, B. Jin, C.W.K. Chow, C. Saint, Water Res. 44 (2010) 2997–3027.
[6] P.G. Wu, R.C. Xie, J.A. Imlay, J.K. Shang, Appl. Catal. B 88 (2009) 576–581.
[7] L. Rizzo, D. Sannino, V. Vaiano, O. Sacco, A. Scarpa, D. Pietrogiacomi, Appl. Catal. B 144 (2014) 369–378.
[8] X.B. Chen, S.S. Mao, Chem. Rev. 107 (2007) 2891–2959.
[9] A. Fujishima, T.N. Rao, D.A. Truk, J. Photochem. Photobiol. C 1 (2000) 1–21.
[10] T.Z. Tong, J.L. Zhang, B.Z. Tian, F. Chen, D.N. He, J. Hazard. Mater. 155 (2008) 572–579.
[11] B.Z. Tian, C.Z. Li, F. Gu, H.B. Jiang, Y.J. Hu, J.L. Zhang, Chem. Eng. J. 151 (2009) 220–227.
[12] R. Asahi, T. Morikawa, T. Ohwaki, K. Aoki, Y. Taga, Science 293 (2001) 269–271.
[13] Y.X. Niu, M.Y. Xing, B.Z. Tian, J.L. Zhang, Appl. Catal. B 2012 (2012) 253–260.
[14] Y. Tian, T. Tatsuma, J. Am. Chem. Soc. 127 (2005) 7632–7637.
[15] W. Zhao, W.H. Ma, C.C. Chen, J.C. Zhao, Z.G. Shuai, J. Am. Chem. Soc. 126 (2004) 4782–4783.
[16] E. Bae, W. Choi, J. Park, H.S. Shin, S.B. Kim, J.S. Lee, J. Phys. Chem. B 108 (2004) 14093–14101.
[17] W.W. Zou, J.L. Zhang, F. Chen, Mater. Lett. 64 (2010) 1710–1712.
[18] P. Wang, B.B. Huang, X.Y. Qin, X.Y. Zhang, Y. Dai, J.Y. Wei, M.H. Whangbo, Angew. Chem. Int. Ed. 47 (2008) 7931–7933.
[19] B.Z. Tian, J.L. Zhang, Catal. Surv. Asia 16 (2012) 210–230.
[20] P. Wang, B.B. Huang, Y. Dai, M.H. Whangbo, Phys. Chem. Chem. Phys. 14 (2012) 9813–9825.
[21] P. Wang, B.B. Huang, X.Y. Zhang, X.Y. Qin, H. Jin, Y. Dai, Z.Y. Wang, J. Wei, J. Zhan, S.Y. Wang, J.P. Wang, M.H. Whangbo, Chem. Eur. J. 15 (2009) 1821–1824.
[22] P.F. Hu, Y.L. Cao, Dalton Trans. 41 (2012) 8908–8912.
[23] R.F. Dong, B.Z. Tian, C.Y. Zeng, T.Y. Li, T.T. Wang, J.L. Zhang, J. Phys. Chem. C 117 (2013) 213–220.
[24] Y.P. Bi, J.H. Ye, Chem. Commun. 43 (2009) 6551–6553.
[25] Y.Y. Li, Y. Ding, J. Phys. Chem. C 114 (2010) 3175–3179.
[26] Z.Z. Lou, B.B. Huang, X.Y. Qin, X.Y. Zhang, H.F. Cheng, Y.Y. Liu, S.Y. Wang, J.P. Wang, Y. Dai, Chem. Commun. 48 (2012) 3488–3490.
[27] J.G. Yu, G.P. Dai, B.B. Huang, J. Phys. Chem. C 113 (2009) 16394–16401.
[28] Y.Q. Yang, G.K. Zhang, W. Xu, J. Colloid Interface Sci. 376 (2012) 217–223.
[29] J. Gao, B.Y. Xu, B.D. Luo, H.L. Lin, S.F. Chen, Appl. Surf. Sci. 257 (2011) 7083–7089.
[30] A.Y. Yin, K.G. Fan, W.L. Dai, J. Hazard. Mater. 211–212 (2012) 77–82.
[31] C. Hu, J. Guo, J.H. Qu, X.X. Hu, Langmuir 23 (2007) 4982–4987.
[32] M.Y. Xing, Y.M. Wu, J.L. Zhang, F. Chen, Nanoscale 2 (2010) 1233–1239.
[33] B.Z. Tian, C.Z. Li, J.L. Zhang, Chem. Eng. J. 191 (2012) 402–409.
[34] L.D. Armelao, D. Barreca, G. Bottaro, Chem. Mater. 16 (2004) 3331–3338.
[35] P. Wang, B.B. Huang, Z.Z. Lou, X.Y. Zhang, X.Y. Qin, Y. Dai, Z.K. Zheng, X.N. Wang, Chem. Eur. J. 16 (2010) 538–544.
[36] B.Z. Tian, T.T. Wang, R.F. Dong, S.Y. Bao, F. Yang, J.L. Zhang, Appl. Catal. B 147 (2014) 22–28.
[37] C. Hu, Y.Q. Lan, J.H. Qu, X.X. Xu, A.M. Wang, J. Phys. Chem. B 110 (2006) 4066–4072.
[38] A. Fujishima, X.T. Zhang, D.A. Tryk, Surf. Sci. Rep. 63 (2008) 515–582.
[39] A. Hagfeldt, H. Lindström, S. Södergren, S. Lindquist, J. Electroanal. Chem. 381 (1995) 39–46.
[40] G.P. Dai, J.G. Yu, G. Liu, J. Phys. Chem. C 115 (2011) 7339–7346.
[41] J.Y. Zhang, Y.H. Wang, J. Jin, J. Zhang, Z. Lin, F. Huang, J.G. Yu, ACS Appl. Mater. Interface 5 (2013) 10317–10324.
[42] J. Zhang, J.G. Yu, M. Jaroniec, J.R. Gong, Nano Lett. 12 (2012) 4584–4589.
[43] C. Hu, T.W. Peng, X.X. Hu, Y.L. Nie, X.F. Zhou, J.H. Qu, H. He, J. Am. Chem. Soc. 132 (2010) 857–862.
[44] X.F. Zhou, C. Hu, X.X. Hu, T.W. Peng, J.H. Qu, J. Phys. Chem. C 114 (2010) 2746–2750.
[45] L.-S. Zhang, K.-H. Wong, H.-Y. Yip, C. Hu, J.M. Yu, C.-Y. Chan, P.-K. Wong, Environ. Sci. Technol. 44 (2010) 1392–1398.
[46] W.H. Ma, Y.P. Huang, J. Li, M.M. Cheng, W.J. Song, J.C. Zhao, Chem. Commun. (2003) 1582–1583.
[47] S. Linic, P. Christopher, D.B. Ingram, Nat. Mater. 10 (2011) 911–921.
[48] T. Morimoto, K. Suzuki, M. Torikoshi, T. Kawahara, H. Tada, Chem. Commun. (2007) 4291–4293.